Extreme dry advection dominates the record-breaking Yangtze River heatwave in midsummer of 2022

Shuai Hu[1], Tianjun Zhou[1, 2*], Dongdong Peng[3], Wanyi Jiang[1, 2], Bo Lu[4], Bo Wu[1], Xiaolong Chen[1], Lixia Zhang[1], Wenxia Zhang[1]

[1] State Key Laboratory of Numerical Modeling for Atmospheric Sciences and Geophysical Fluid Dynamics, Institute of Atmospheric Physics, Chinese Academy of Sciences, Beijing, China

[2] College of Earth and Planetary Sciences, University of Chinese Academy of Sciences, Beijing, China

[3] Institute of Tropical and Marine Meteorology, China Meteorological Administration, Guangzhou, China

[4] National Climate Center, China Meteorological Administration, Beijing, China

Corresponding author: Tianjun Zhou (zhoutj@lasg.iap.ac.cn)

Key Points:

- The SAT anomaly averaged over the YRV in midsummer of 2022 is 1.98°C, 72.7% of which is contributed by the interannual variability.
- Surface short-wave cloud radiative forcing associated with anomalous descending flows is the key process in driving the 2022 YRV heatwave.
- The anomalous descending motions over the YRV in midsummer of 2022 are caused by the extreme dry air advection.

Abstract

The Yangtze River Valley (YRV) experienced an unprecedented heatwave in midsummer of 2022, but the detailed physical processes involved in the influence of anomalous large-scale atmospheric circulation on the heatwave remain unknown. Here, we show that the positive meridional gradient of anomalous atmospheric moisture at the middle-lower troposphere and associated extreme dry air advection over the YRV are key prerequisites for the formation of the 2022 YRV heatwave. The 2022 YRV heatwave is dominated by the interannual variability, which contributes 72.7% to the total temperature anomalies. Diagnosis of the surface heat budget equation indicates that the surface cloud radiative forcing is the most important process in driving the 2022 YRV heatwave, which is dominated by the positive surface short-wave cloud radiative forcing associated with the suppressed precipitation and the middle-low clouds. The suppressed precipitation is induced by the vertical dynamical processes of anomalous moisture advection caused by the anomalous descending flows over the YRV, which are driven by the negative advection of anomalous latent heat energy by climatological meridional wind (anomalous dry air advection) according to the atmospheric moist static energy equation. Simulations from the Lagrangian model FLEXPART further indicate that the moisture anomaly over the north of YRV is mainly originated from the surface evaporation in the YRV, implying that there is a positive land-air feedback during the life cycle of the YRV heatwave. Our study adds a perspective to the existing mechanism analyses of the 2022 YRV heatwave to serve accurate climate prediction and adaptation planning.

1 Introduction

During the boreal midsummer (July-August) of 2022, the Yangtze River Valley (YRV) experienced an unprecedented intense, and prolonged heatwave, with the maximum temperature exceeding 40°C (R. Lu et al., 2023; Mallapaty, 2022). The extreme YRV heatwave was followed by a worst hydrologic drought (Ma et al., 2022) and eventually led to a severe compound extreme, imposing great impacts on human health, agriculture, water and energy supplies (Yuan et al., 2023). The severity of the 2022 YRV extreme heatwave highlights the importance of unraveling the underlying mechanisms to serve accurate climate prediction and adaptation planning.

Abnormal large-scale atmospheric circulation background and its associated lower boundary conditions are the key prerequisites for the occurrence and maintenance of extreme climate events (Ha et al., 2022; W. Wang et al., 2014), and several efforts have been devoted to understanding the formation process of the large-scale circulation background associated with the 2022 YRV heat event (Tang et al., 2023; Z. Wang et al., 2023; Zhang et al., 2023). It is generally acknowledged that the merged subtropical high belt over the Asian continent is critical to the 2022 YRV heat event, which is a consequence of the synergistic effects of the westward extension of the low-level western North Pacific subtropical high (WNPSH) and the eastward extension of the upper-level South Asian high (SAH) (Chen & Li, 2023). The merge of the two subtropical high systems formed initially in July, and intensified in August (Zhang et al., 2023). In July of 2022, the extraordinary circulation anomalies are suggested to be driven by the diabatic heating associated with the flooding in Pakistan (Z. Wang et al., 2023), the La Niña SSTA pattern (Tang et al., 2023), the enhanced convection over the tropical eastern Indian Ocean (Chen & Li, 2023), and the atmospheric intraseasonal oscillation (Liu et al., 2023). While in August, the negative phase of the Silk Road pattern (SRP) (Enomoto et al., 2003; R.-Y. Lu et al., 2002) cooperates with the above processes to intensify the circulation anomalies (Z. Wang et al., 2023; Zhang et al., 2023). In addition, the role of local land–air feedback caused by the dry soil moisture in the 2022 YRV heatwave was also emphasized (Jiang et al., 2023), which can amplify the heatwave by reducing the evapotranspiration and increasing the upward sensible flux (Erdenebat & Sato, 2018; Thompson et al., 2022).

The existing studies commonly assumed that the heatwave was driven by large-scale anomalous anticyclonic circulation via adiabatic heating from descending flows and

enhancement of incoming solar radiation, but the detailed processes are seldom investigated. What is the relationship between the large-scale circulations and the extreme 2022 YRV heatwave? What are the detailed physical processes underlying the formation of descending motions over the YRV? This study aims to answer these two questions via rigorous diagnostic analysis. The remainder of the paper is outlined as follows. Observational datasets and analytical methods are introduced in section 2. Section 3 investigates the detailed physical processes responsible for the 2022 YRV heatwave. The concluding remarks are given in section 4.

2 Data and Methods

2.1. Observations

In this study, we used the atmospheric reanalysis of surface air temperature (SAT), surface short-wave/long-wave radiations, surface sensible/latent fluxes, cloud cover, atmospheric circulations, precipitation, and evaporation from the European Centre for Medium-Range Weather Forecasts reanalysis (ERA5) with a horizontal resolution of 0.25°×0.25° (Hersbach et al., 2020). The SST data is derived from the National Oceanic and Atmospheric Administration Extended Reconstructed SST version 5 (ERSSTv5) dataset (Huang et al., 2015).

2.2 Analytical method

To investigate the physical processes responsible for the 2022 YRV heatwave, we diagnose the linearized surface heat budget equation (J. Lu & Cai, 2009), which can be written as:

$$\Delta T \approx \frac{1}{4\sigma\bar{T}_s^3}\Delta F^{\uparrow} = \frac{1}{4\sigma\bar{T}_s^3}[-(\Delta\alpha)(\overline{S^{\downarrow}} + \Delta S^{\downarrow}) + \Delta CRF_s + (1-\bar{\alpha})\Delta S^{\downarrow,clr} + \Delta F^{\downarrow,clr} - \Delta Q - \Delta(H+LE)] \quad (1)$$

where T is the surface temperature. $F^{\downarrow}$ and $F^{\uparrow}$ are surface downward and upward long-wave (LW) radiations with $F^{\uparrow} \approx \sigma T_s^4$ according to Stefan-Boltzmann law. $S^{\downarrow}$ and $S^{\uparrow}$ are surface downward and upward short-wave radiations. α is the surface albedo, which can be derived from the ratio of of $S^{\uparrow}$ to $S^{\downarrow}$ at surface. $(\cdot)^{clr}$ represents the surface clear-sky radiations. H and LE are surface sensible and latent heat fluxes. Q is the heat storage term. The overbar denotes the unperturbed mean climate state, and the Δ represents the perturbation relative to the mean climate state. The terms on the RHS of Eq. (1) represent six different processes with effect on temperature change, including the surface albedo feedback (SAF), the change in surface cloud radiative forcing (ΔCRF_s), the non-SAF-induced change in clear-sky shortwave radiation, the

change in downward clear-sky longwave radiation fluxes, the change in heat storage, and the changes in surface sensible/latent fluxes, respectively.

The ΔCRF_s with the SAF excluded can be decomposed into two terms as:

$$\Delta CRF_s = (1-\bar{\alpha})\Delta S^{\downarrow,cld} + \Delta F^{\downarrow,cld} \quad (2)$$

where $(\cdot)^{cld}$ is the difference between the surface total-sky radiation and the surface clear-sky radiation, which represents the cloud radiative forcing. $\bar{\alpha}$ is the surface albedo of the unperturbed mean climate state.

To understand the physical processes governing the variations of YRV midsummer rainfall, following (Chou et al., 2013) and (Hu et al., 2021), the linearized column-integrated atmospheric moisture flux equation was diagnosed as follows:

$$P' = E' - <\bar{\boldsymbol{V}}\cdot\nabla_h q'> - <\bar{\omega}\cdot\partial_p q'> - <\boldsymbol{V}'\cdot\nabla_h\bar{q}> - <\omega'\cdot\partial_p\bar{q}> + NL + Residual \quad (3)$$

where q is specific humidity, $\boldsymbol{V}$ is horizontal wind, ω is vertical pressure velocity, P is precipitation, E is surface evaporation and the angle bracket $<>$ denotes the mass-weighted vertical integral through the entire atmospheric column. t, h and p represent the time dimension, horizontal and vertical direction, respectively. The NL is the nonlinear component, and the $Residual$ denotes the residual term. The overbars (primes) represent the climatological monthly mean (the monthly anomaly).

To investigate the mechanisms responsible for the anomalous vertical motion, the linearized column-integrated moist static energy (MSE) equation (Neelin & Held, 1987; Wu et al., 2017) was diagnosed as follows:

$$<\omega'\partial_p\bar{h}> \approx F'_{net} - <u'\partial_x\overline{(C_pT+L_vq)}> - <\bar{u}\partial_x(C_pT+L_vq)'> - <v'\partial_y\overline{(C_pT+L_vq)}> - <\bar{v}\partial_y(C_pT+L_vq)'> - <\bar{\omega}\partial_p h'> + NL \quad (4)$$

where F_{net} represents the net flux into the atmospheric column. The h denotes the MSE, which can be written as $h = C_pT + L_vq + \phi$. The $(C_pT + L_vq)$ is the moist enthalpy. C_P and L_v are the specific heat at constant pressure and the latent heat of vaporization, respectively; T denotes the air temperature; q is the specific humidity; ϕ denotes the geopotential; u, v and ω represent the zonal wind, meridional wind and vertical velocity, respectively; x, y and p represent the zonal, meridional and vertical direction, respectively. The NL is the nonlinear component. The overbars (primes) represent the climatological monthly mean (the monthly anomaly). The angle bracket $<>$ denotes the mass-weighted vertical integral through the entire atmospheric column. The

negative terms on the righthand side of Eq. (4) can drive anomalous descending motion under the constraints of the MSE budget balance (Biasutti et al., 2018).

The atmospheric precipitable water vapor (PW) and the vertically integrated moisture flux (Q) (Zhou & Yu, 2005) were calculated as

$$PW = \frac{1}{g}\int_{100}^{p_s} q dp \tag{5}$$

$$Q = \frac{1}{g}\int_{100}^{p_s} q\boldsymbol{V} dp \tag{6}$$

where q is specific humidity; $\boldsymbol{V}$ is horizontal wind vector; p is pressure, p_s is surface pressure, and g is the acceleration due to gravity.

To identify the geographical moisture source regions of the anomalous atmospheric moisture accumulations over the region to the north of YRV in midsummer of 2022, we employed the Lagrangian model FLEXPART v9.2. The FLEXPART model was developed by the Norwegian Institute for Air Research, which can be used to accurately describe the moisture-transporting processes associated with atmospheric vapor by analyzing the trajectories of corresponding air particles. In this study, the FLEXPART simulations were conducted forward in time with the "domain fill" option for midsummer during 1979–2022 based on the 6-hourly Climate Forecast System Reanalysis (CFSR). The details of setting options used in the FLEXPART simulations can be referred to (Peng et al., 2022; Peng et al., 2020). The moisture source contributions for the atmospheric vapor are quantified based on the method from (Sodemann et al., 2008) by tracking all the air particles over the target region.

The monthly anomalies were obtained by removing the mean monthly climatology of the period 1991–2020. The interannual variability is estimated by the difference between the original anomalies and the 9-year moving average. The long-term linear trend is estimated by the linear trend of the 9-year moving average, and the interdecadal variability is represented by the difference between the 9-year moving average and the long-term linear trend.

3 Results

3.1 The 2022 YRV heatwave and its associated circulation anomalies

The maximal surface warmings associated with the 2022 midsummer YRV heatwave exhibit a zonally elongated structure, spanning from the northern Tibetan Plateau to the entire YRV (Fig. 1a). The area-averaged SAT anomalies over the YRV in midsummer of 2022 relative

to the 1991–2020 climatology is 1.98°C, which sets the highest record for the period 1960-2022 (Fig. 1b). The SAT anomalies over the YRV in 2022 involve signals with different timescale, including the long-term linear trend, the interdecadal variability, and the interannual variability. Estimations of their relative contribution show that the 2022 YRV heatwave is dominated by the component of interannual variability, which contributes 1.44°C to the total temperature anomalies in midsummer of 2022, accounting for 72.7% of the anomaly amplitude.

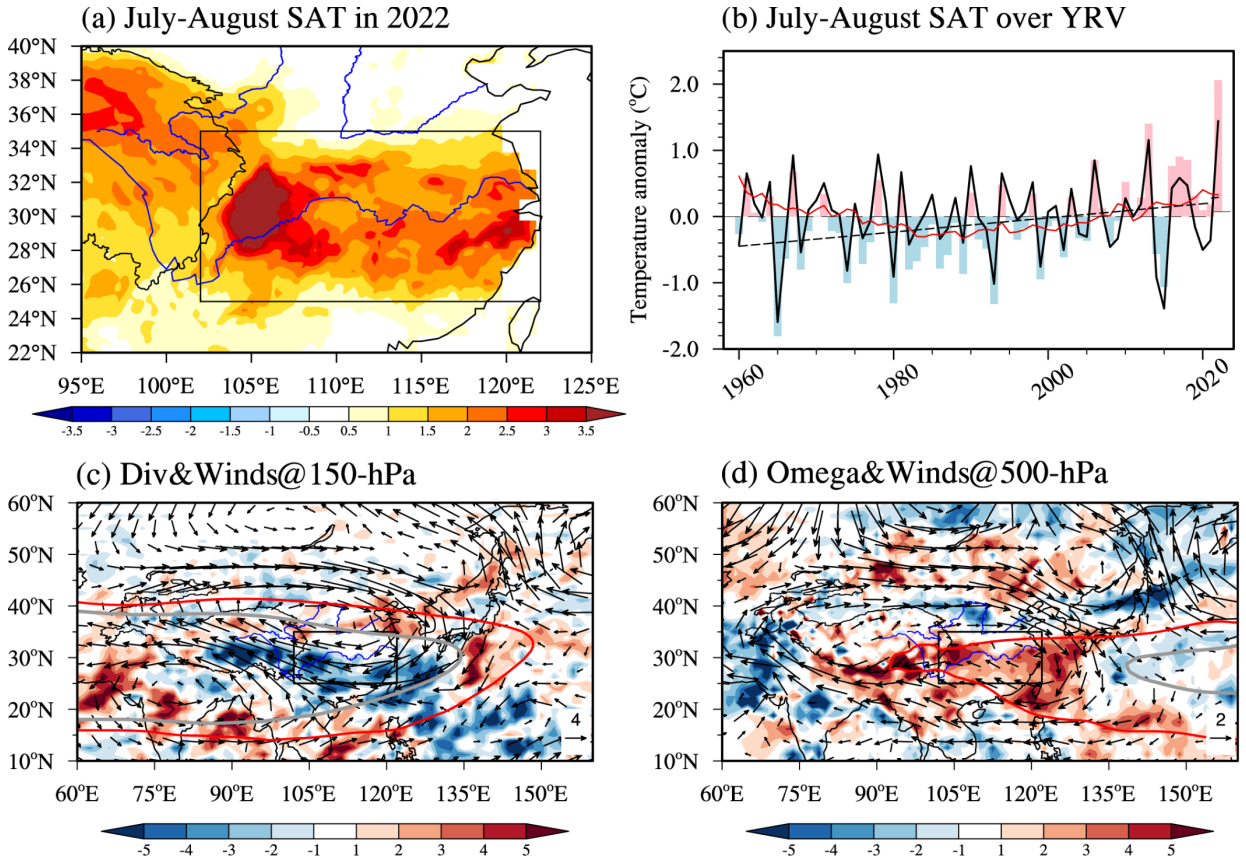

Figure 1. The 2022 midsummer (June-July) heatwave in the Yangtze River Valley (YRV) and its associated circulation anomalies. (a) July-August mean surface air temperature (SAT) anomalies in 2022, unit: °C. The SAT anomalies are relative to the period of 1991–2020. (b) Time series of the July-August mean SAT anomalies averaged over the YRV from 1960 to 2022. The original SAT anomalies, and the components of linear trend, interdecadal variability, and interannual variability are represented by bar, dashed black line, red line, and solid black line, respectively. (c) July-August mean atmospheric divergence (shading, unit: 10^{-6} s^{-1}) and horizontal winds (vector, unit: $m \cdot s^{-1}$) anomalies at 150-hPa. The July-August mean South Asian high (SAH) at 150-hPa is denoted by the 14300 gpm contour of geopotential height. (d) July-August mean vertical pressure velocity (shading, unit: $Pa \cdot s^{-1}$) and horizontal

177 winds (vector, unit: $m \cdot s^{-1}$) anomalies at 500-hPa. In (c, d), the July-August mean South Asian high (SAH)
178 at 150-hPa and western Pacific subtropical high (WPSH) at 500-hPa are denoted by the 14300 gpm and
179 5880 gpm contour of geopotential height, respectively, where the gray line represents the climatology for
180 the period of 1991–2020, and the red line represents the case in 2022. The black boxes in (a, c, d) denote
181 the YRV (25°-35°N,102°-122°E).

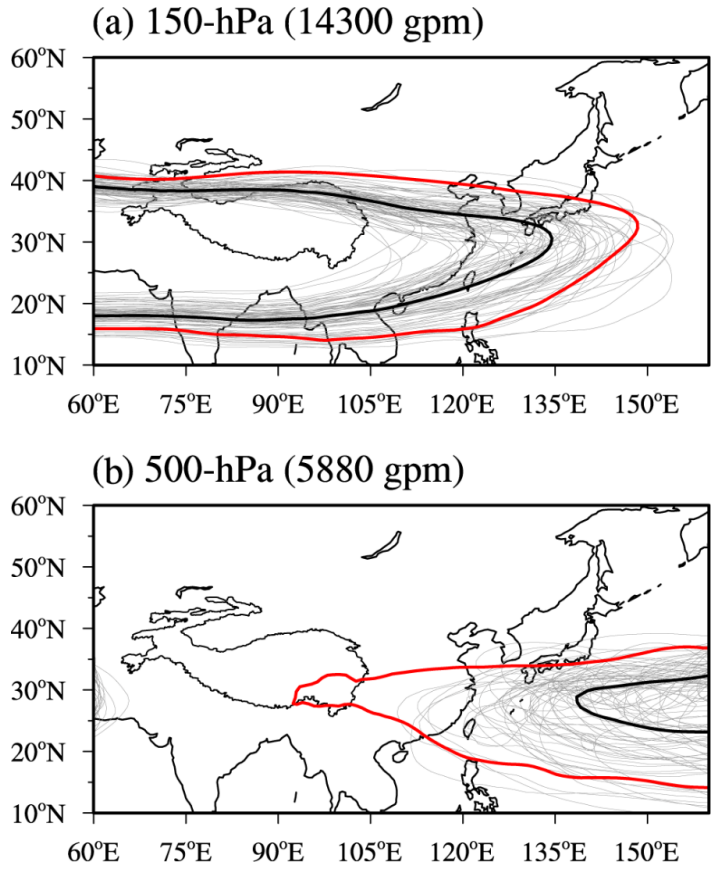

182

183 **Figure 2. The anomalous western North Pacific subtropical high (WNPSH) and the South Asian**
184 **high (SAH) in midsummer of 2022.** (a) The July-August mean SAH at 150-hPa denoted by the 14300
185 gpm contour of geopotential height. (b) The July-August mean WPSH at 500-hPa denoted by the 5880
186 gpm contour of geopotential height. The bold black lines represent the climatology for the period of
187 1991–2020. The red and light gray lines represent the cases in 2022 and other years, respectively.

188 The circulation anomalies associated with the extreme heatwave in midsummer 2022 are the
189 eastward shift of the SAH in the upper troposphere (Fig. 1c), and the westward extension of the
190 WNPSH in the middle-lower troposphere (Fig. 1d). Although the border of the SAH in
191 midsummer of 2022 lies within the range of historical variations for the period 1960-2022, the
192 westward extension of the WNPSH in the 500-hPa level breaks the record held since the year

1960 (Fig. 2). The overlaps of the two subtropical high systems produce an anomalous anticyclone in the middle to upper troposphere over the YRV, accompanied by atmospheric divergence and descending motion along the southern edge of the anomalous anticyclone. It is generally acknowledged that high-pressure circulation systems can induce descending motion and favor the occurrence of heat waves. The westward shift of the WNPSH covers the whole YRV and a large part of the Western North Pacific, while the anomalous descending motions only occur at the upper and lower reaches of YRV and the adjacent sea (Fig. 1d). How does the anomalous descending motions over the YRV come into existence in midsummer of 2022? What are the detailed mechanisms underlying the influence of the anomalous descending motions on the extreme YRV heatwave? We will address these questions in the following analyses.

3.2 Budget analysis for the 2022 YRV heatwave

To quantitatively evaluate the contributions of different processes to the 2022 YRV heatwave, the surface heat budget equation [Eq. (1)] was diagnosed on the interannual time scale. The sum of the six terms on the right-hand side of Eq. (1) reasonably reproduces the 2022 YRV heatwave, with the area-averaged surface temperature anomalies over the YRV resulting from six feedback processes reaching 1.74 °C (Fig. 3a). The budgets also can reproduce the interannual variability of the midsummer SAT anomalies for the period 1960-2022, with the correlation coefficient reaching 0.96 (Fig. 3b). These results suggest that the budget of surface heat budget equation are reliable in term of representing the midsummer SAT variations over the YRV.

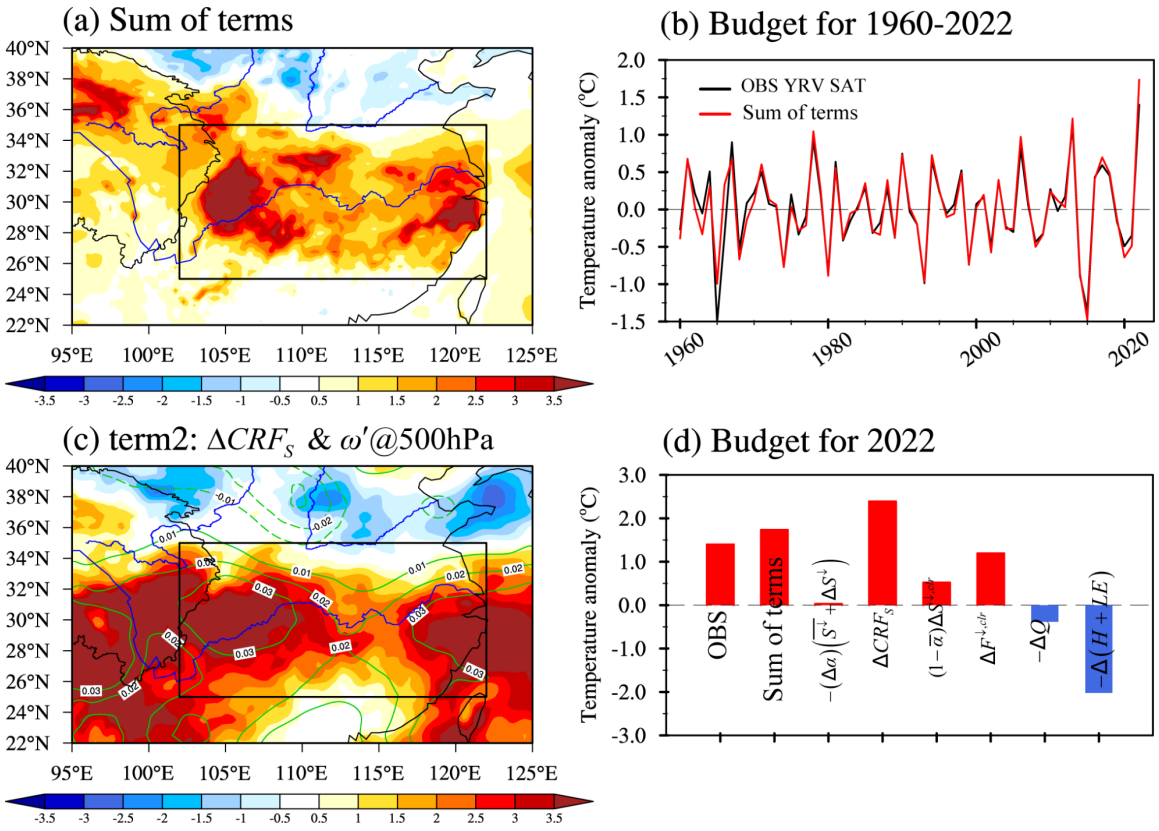

Figure 3. Budget analysis of the surface heat budget equation [Eq. (1)] for the 2022 midsummer heat wave in the YRV. (a) the sum of the six terms on the right-hand side of Eq. (1). Unit: °C. (b) budget for the interannual variability of the July-August mean YRV SAT anomalies for the period 1960-2022. The red (black) line represents the sum of the six budget terms (observed YRV SAT), respectively. The blue line represents the standardized vertical velocity anomaly at 500-hPa averaged over the YRV. (c) the SAT anomalies contributed by the change in surface cloud radiative forcing (ΔCRF_S) (shading, unit: °C), and vertical velocity anomaly at 500-hPa (contour, unit: Pa·s^{-1}, the interval is 0.01). (d) the partial changes from six individual feedback processes to the positive surface temperature anomalies associated with the 2022 YRV heatwave. From left to the right in the abscissa: the SAT anomalies averaged over the YRV for the observation (OBS), the sum of the six terms, and contributions from the surface albedo feedback, the change in ΔCRF_S, the non-SAF-induced change in clear-sky shortwave radiation, the change in downward clear-sky longwave radiation fluxes, the change in heat storage, and the changes in surface sensible/latent fluxes, respectively. Unit: °C. The black boxes in (a, c) denote the YRV (25°-35°N,102°-122°E).

The partial changes from individual feedback processes to the positive surface temperature anomalies associated with the 2022 YRV heatwave are quantitatively estimated in Fig. 3d. Among these processes, the surface cloud radiative forcing (ΔCRF_S) is the most important

process, which contributes 2.39°C to the total anomalies. The ΔCRF_s can be further decomposed into two terms, the surface short-wave CRF and the surface long-wave CRF according to Eq. (2). As shown in Fig. 4, the ΔCRF_s is dominated by the surface short-wave CRF (Fig. 4a, b), which spatial distributions resemble the anomalies of precipitation and middle and low clouds (Fig. 4c, d). When the precipitation is suppressed, the associated decreased middle and low clouds lead to increased surface incoming short-wave radiations, which further drive the surface warmings. So, the next question is why the precipitation over the YRV was suppressed in midsummer of 2022.

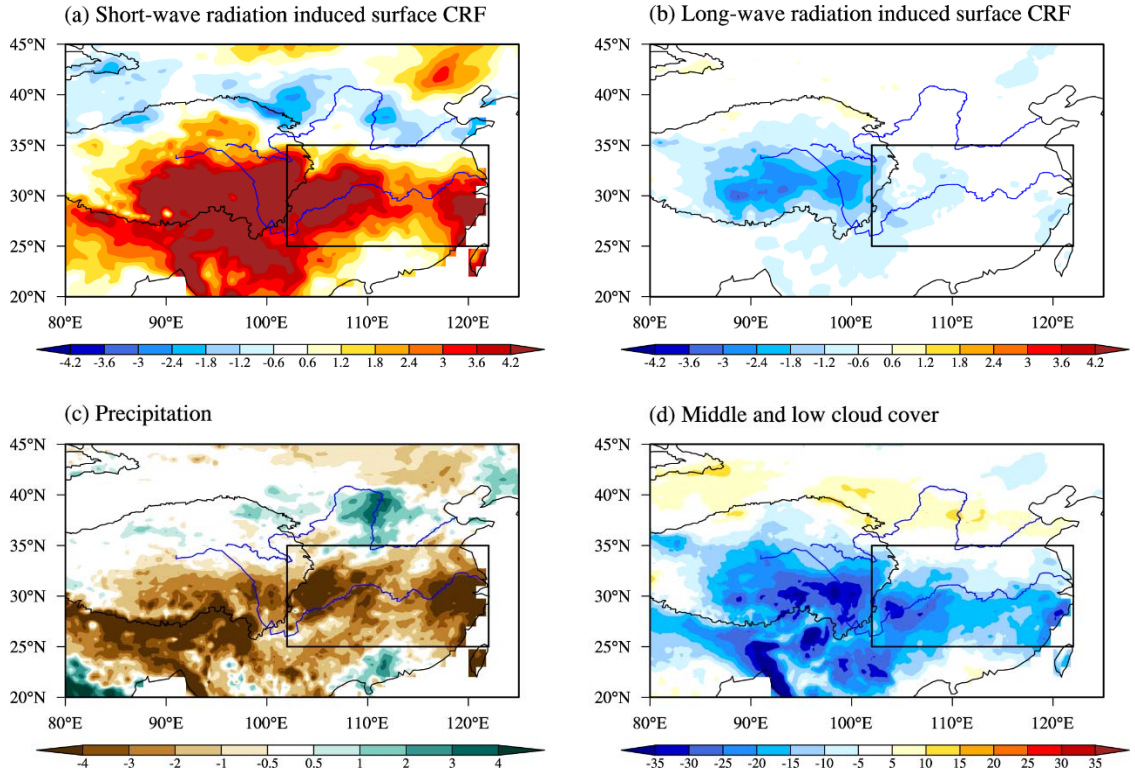

Figure 4. Formation processes of the surface cloud radiative forcing in midsummer of 2022. (a, b) the July-August mean surface cloud radiative forcing induced by the surface short-wave radiation (a), and the surface long-wave radiation (b), unit: °C. (c, d) the July-August mean precipitation (unit: mm·day^{-1}) (d), and the middle and low cloud cover (unit: %).

According to the atmospheric moisture budget analysis, the negative precipitation anomalies are dominated by the vertical dynamical processes of anomalous moisture advection ($-<\omega' \cdot \partial_p \bar{q}>$) (Fig. 5 and 6). Quantitatively, the precipitation anomalies averaged over the YRV is -2.32 mm/day, with the contribution from $-<\omega' \cdot \partial_p \bar{q}>$ reaching -2.12 mm/day, accounting for 91% of the precipitation variations. The $-<\omega' \cdot \partial_p \bar{q}>$ is linked dynamically

247 with the anomalous vertical velocity, and the descending motion at 500 hPa over the YRV well
248 coincides with the $-<\omega' \cdot \partial_p \bar{q}>$ (Fig. 6). Hence, the spatial pattern of the ΔCRF_s is also in
249 accord with the descending motion at 500 hPa, which isoline of 0.03 Pa·s-1 well coincides with
250 the maximum values of ΔCRF_s and SAT anomalies (Fig. 2c). The interannual variations of
251 midsummer SAT anomalies in the YRV during 1960-2022 is also closely related with the area-
252 averaged anomalous vertical velocity at 500 hPa over the YRV, with the correlation coefficient
253 reaching 0.59 ($p<0.01$) (not shown). The results suggest that the anomalous descending motion is
254 associated with the YRV heatwave through the surface short-wave CRF, which is dynamically
255 linked with the changes in precipitation and cloud cover.

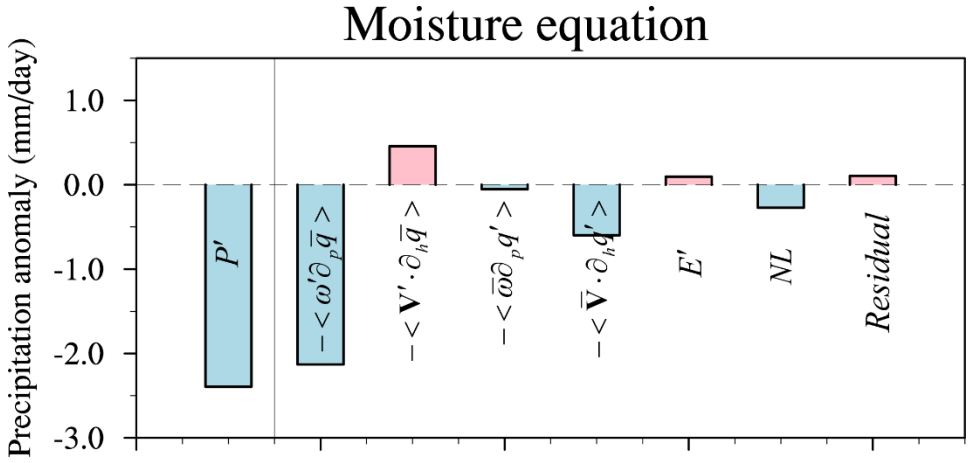

256

257 **Figure 5.** Budget analysis for the moisture equation [Eq. (3), units: mm·day^{-1}] for the 2022 midsummer
258 in the YRV (25°-35°N,102°-122°E).

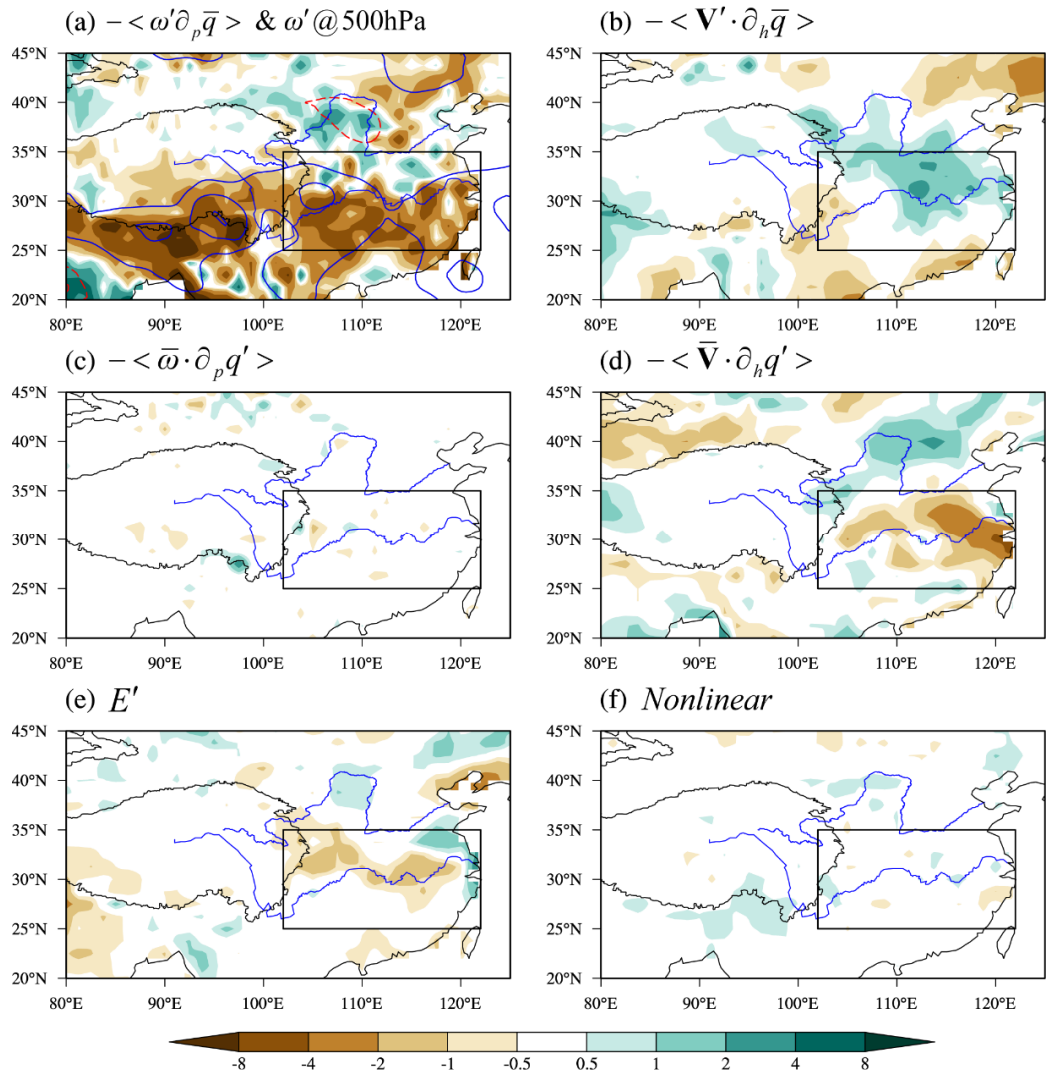

Figure 6. Budget analysis of the column-integrated atmospheric moisture flux equation [Eq. (3)] for the 2022 midsummer in the YRV. (a) the vertical dynamic component of the vertically integrated moisture advection term ($-<\omega'\partial_p\bar{q}>$) and the anomalous vertical pressure velocity at the 500 hPa. (b) the horizontal dynamic component of the vertically integrated moisture advection term ($-<\boldsymbol{V}'\cdot\nabla_h\bar{q}>$). (c) the vertical thermodynamic component of the vertically integrated moisture advection terms ($-<\bar{\omega}\cdot\partial_p q'>$), (d) the horizontal thermodynamic component of the vertically integrated moisture advection terms ($-<\bar{\boldsymbol{V}}\cdot\nabla_h q'>$), (e) the surface evaporation term (E'), and (f) the nonlinear components. The units of the vertically integrated moisture advection term and anomalous vertical pressure velocity are mm·day^{-1} and Pa·s^{-1}. The black boxes denote the YRV (25°-35°N,102°-122°E).

In midsummer of 2022, the anomalous descending motion at 500 hPa over the YRV at interannual timescales is the strongest since 1960. What are the formation processes of the anomalous vertical motions? We further diagnosed the MSE equation [Eq. (4)] to the regions with the 500 hPa vertical velocity anomalies above 0.03 Pa·s^{-1}. The column-integrated MSE equation can accurately represent the 500 hPa vertical velocity anomalies above these regions for the period of 1960-2022 (Fig. 7b). For the midsummer of 2022, the budget results suggest that the anomalous descending motions were driven by the anomalous negative advection of anomalous moist enthalpy by climatological meridional wind ($-<\bar{v}\partial_y\left(C_pT+L_vq\right)'>$), and the anomalous meridional dry air advection ($-<\bar{v}\partial_y(L_vq)'>$) has the largest contributions (Fig. 7a). The $-<\bar{v}\partial_y(L_vq)'>$ in 2022 is also the strongest since 1960, consistent with the extreme anomalous descending motions (Fig. 7b).

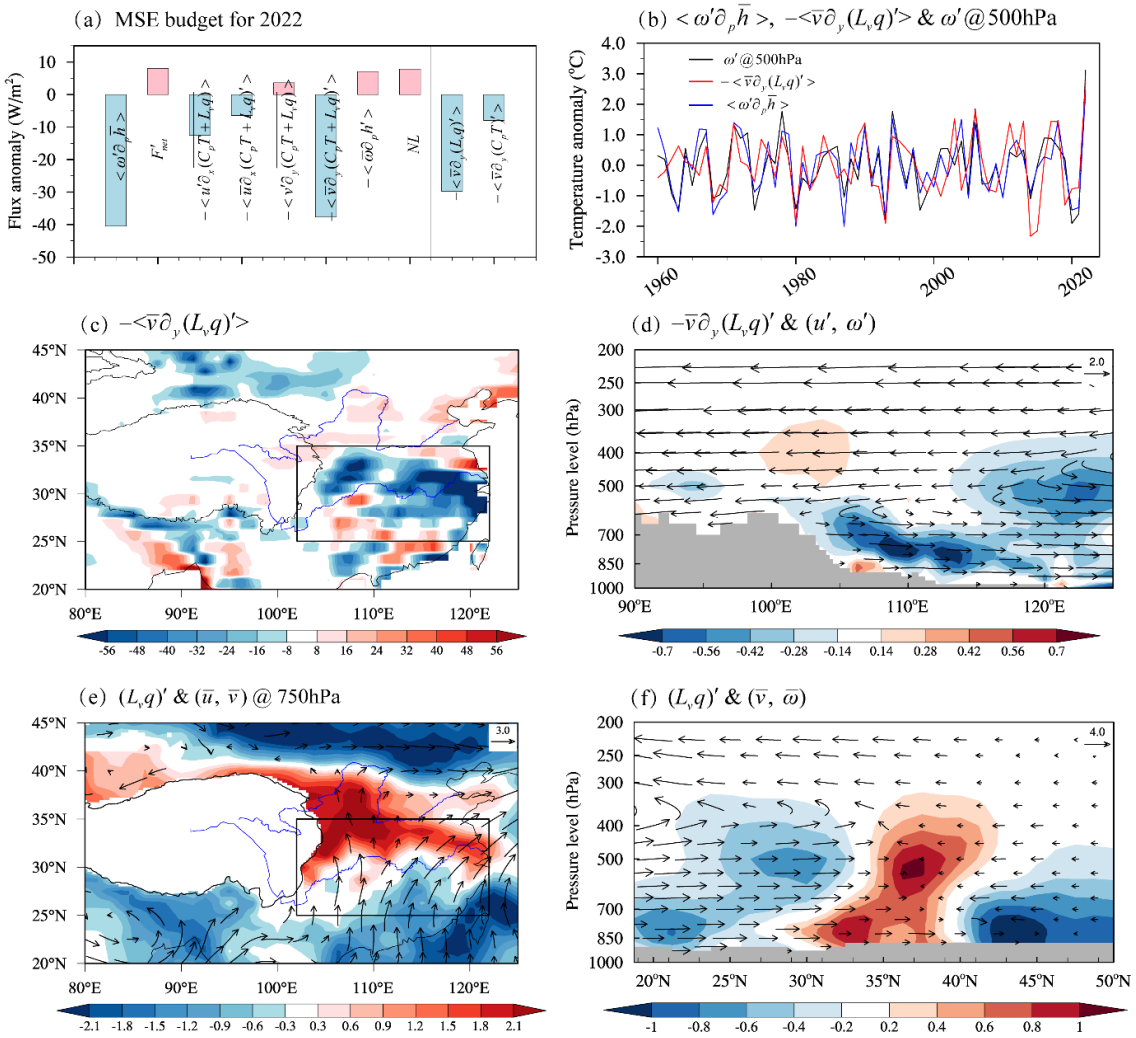

Figure 7. Budget analysis of column-integrated moist static energy (MSE) equation [Eq. (4)] for the anomalous vertical velocity over the YRV. (a) Each budget term of the MSE equation for the anomalous vertical velocity over the YRV in midsummer of 2022. Unit: $W \cdot m^{-2}$. The budget is conducted to the regions within the YRV where the 500 hPa vertical velocity anomalies above 0.03 $Pa \cdot s^{-1}$. (b) the anomalous vertical velocity at 500 hPa (black line), the vertically integrated anomalous vertical advection of climatological mean MSE ($< \omega' \partial_p \bar{h} >$, red line), and the vertically integrated anomalous meridional advection of anomalous latent heat energy by climatological wind ($- < \bar{v} \partial_y (L_v q)' >$, blue line) averaged over the regions of MSE budget for the period 1960-2022. The time series are standardized. (c) the spatial pattern of $- < \bar{v} \partial_y (L_v q)' >$ in the midsummer of 2022, unit: $W \cdot m^{-2}$. (d) the longitude–height cross section of $-\bar{v} \partial_y (L_v q)'$ (unit: 10^{-3} $J \cdot kg^{-1} \cdot s^{-1}$) and anomalous zonal and vertical winds (unit: $m \cdot s^{-1}$). (e) the spatial pattern of anomalous latent heat energy (unit: 10^3 $J \cdot kg^{-1}$) and climatological horizontal winds at 750-hPa (unit: $m \cdot s^{-1}$). (f) the latitude–height cross-section of the anomalous latent heat energy (shading, unit: 2×10^3 $J \cdot kg^{-1}$) and the climatological meridional and vertical winds (vector, unit: $m \cdot s^{-1}$). The black boxes in (c and e) denote the YRV (25°-35°N, 102°-122°E).

The $- < \bar{v} \partial_y (L_v q)' >$ in 2022 has negative value centers over the YRV (Fig. 7c), and this negative moist enthalpy advection decreases the atmospheric moist static energy and facilitate suppressed local convection under the constraints of the MSE budget balance. From the longitude–height cross section averaged over the YRV, the maximum anomalies of $-\bar{v} \partial_y (L_v q)'$ emerge at the levels between 850 and 700 hPa over the YRV, directly corresponded with the anomalous descending motions at these levels (Fig. 7d). We utilized the 750hPa level to investigate the formation of $- < \bar{v} \partial_y (L_v q)' >$. It can be found that there are positive latent heat energy anomalies over the region between the Yangtze and Yellow River, and negative latent heat energy anomalies over the northern South China Sea, which result in a positive meridional gradient of anomalous latent heat energy ($\partial_y (L_v q)'$) over the YRV (Fig. 7e). Under the background of the climatological East Asian summer monsoon circulations, the negative $-\bar{v} \partial_y (L_v q)'$ is thus generated. The latitude–height cross section of latent heat energy anomalies also indicates that the positive $\partial_y (L_v q)'$ is mainly determined by the meridional gradient of anomalous atmospheric moisture at the middle-lower troposphere (Fig. 7f), and the atmospheric moisture accumulation to the north of YRV plays an important role. Hence, it is vital to investigate the abnormal atmospheric moisture transportation in midsummer of 2022 to understand the formation of the extreme meridional dry air advection.

3.3 Abnormal moisture transportation in midsummer of 2022

The atmospheric precipitable water vapor and the vertically integrated moisture flux anomalies in midsummer of 2022 are shown in Fig. 8a. The most prominent feature is that the atmospheric moisture unusually accumulates to the north of YRV, with less moisture on both the north and south sides. The anomalous moisture accumulations are closely associated with the anticyclonic moisture flux anomalies above South China and the southward moisture flux anomalies above North China (Fig. 8a), implying the key role of large-scale circulations. The vertical profiles of moisture to the north of YRV distribute along the high-pressure ridge line (Fig. 8b), which indicates that the merge of the SAH and WNPSH over the YRV plays an important role in anomalous moisture transportations. According to previous study, the merge of the SAH and WNPSH in midsummer of 2022 could be driven by the diabatic heating associated with the flooding in Pakistan (Z. Wang et al., 2023), the La Niña SSTA pattern (Tang et al., 2023), the enhanced convection over the tropical eastern Indian Ocean (Chen & Li, 2023), the atmospheric intraseasonal oscillation (Liu et al., 2023), and the negative phase of the SRP (Z. Wang et al., 2023).

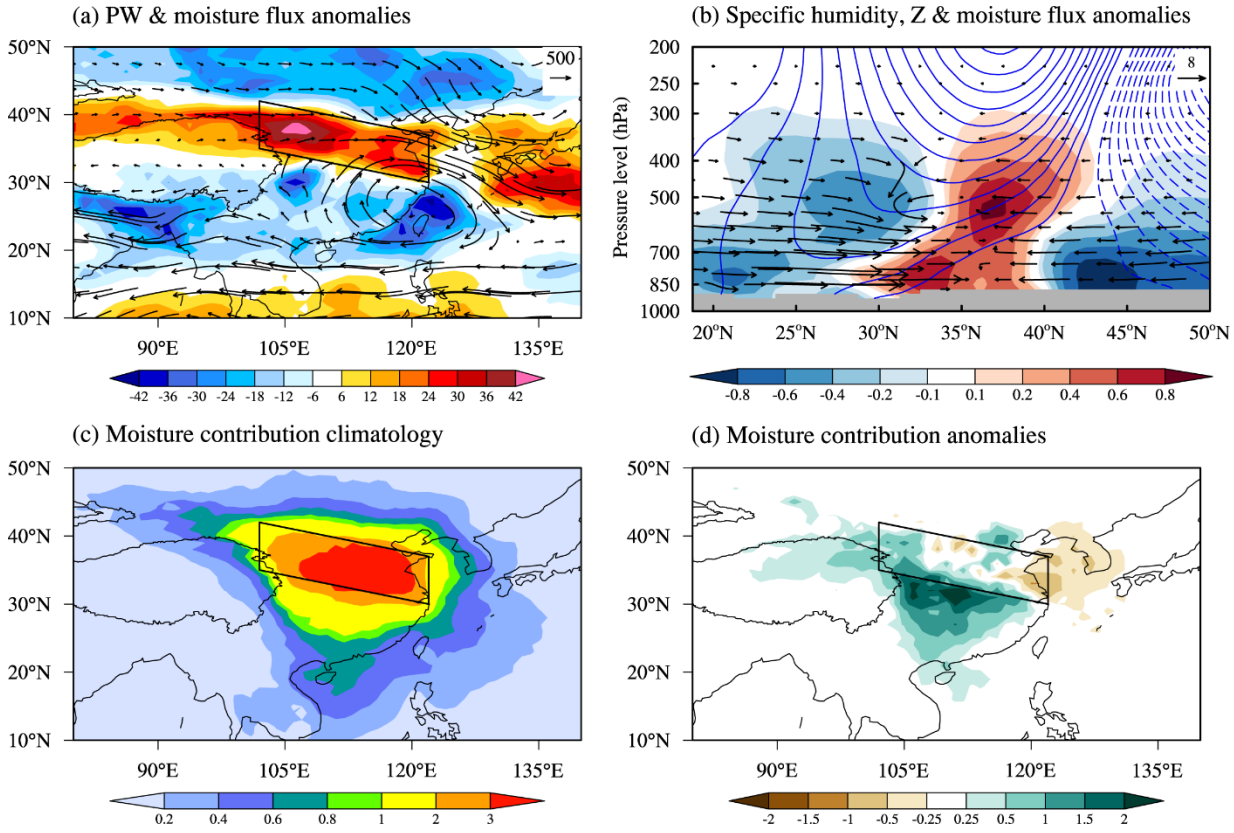

Figure 8. The anomalous atmospheric moisture transportations in midsummer of 2022. (a) the atmospheric precipitable water vapor (PW; shading, unit: $kg \cdot m^{-2}$) and the vertically integrated moisture flux (Q; vector, unit: $kg \cdot m \cdot s^{-1}$) anomalies in midsummer of 2022. (b) the latitude–height cross-section of the moisture flux (vector, unit: $g \cdot m \cdot s^{-1} \cdot kg^{-1}$), specific humidity (shading, unit: $g \cdot kg^{-1}$), and geopotential (contour, unit: $m^2 \cdot s^{-2}$) anomalies in midsummer of 2022 averaged along 102°-122°E. (c) the moisture contribution associated with climatological mean midsummer atmospheric water contents for the region to the north of YRV (black box) derived from all the target back-tracking trajectories over days 10–1 in the FLEXPART simulations. Unit: 10^{11} kg. (d) as in (c), but for the moisture contribution associated with midsummer of 2022.

The moisture contribution associated with climatological mean midsummer atmospheric water contents for the region to the north of YRV (black box in Fig. 8a) over the whole 10-day back-tracking period derived from the FLEXPART simulations are shown in Fig. 8c. The highest center of moisture contribution occurs at the north of YRV, implying that the local evaporation is the main contributor to the atmospheric moisture over the north of YRV (Fig. 8c). With respect to the climate mean, the distributions of moisture contribution anomaly of the midsummer in 2022 show that there are increments in moisture contribution over the middle and upper reaches of the YRV but decrements in moisture contribution over the Yellow Sea (Fig. 8d), which indicate that the atmospheric moisture anomaly over the north of YRV mainly originate from the YRV.

The above analyses suggest that there could be a positive feedback between the heatwave and the atmospheric circulation through anomalous moisture transportation during the 2022 YRV heatwave. When the YRV heatwave develops, the local evaporation is enhanced and thus produces more atmospheric moisture. The increased atmospheric moisture is further transported to the north of YRV by the high-pressure circulation systems, and results in meridional dry air advection over the YRV, which further intensifies the YRV heatwave through the formation of descending motions and associated surface cloud radiative forcing.

4 Conclusion and discussion

In this study, we investigated the detailed physical processes involved in the influence of atmospheric circulation on the 2022 YRV heatwave. Based on the linearized surface heat budget equation, column-integrated atmospheric moisture flux, and moist static energy equation, the key processes to the 2022 YRV heatwave are identified. The schematic of the mechanisms

359 responsible for the influence of extreme dry advection on the record-breaking Yangtze River
360 heatwave in midsummer of 2022 is given in Fig. 9. The main conclusions are listed as follows:

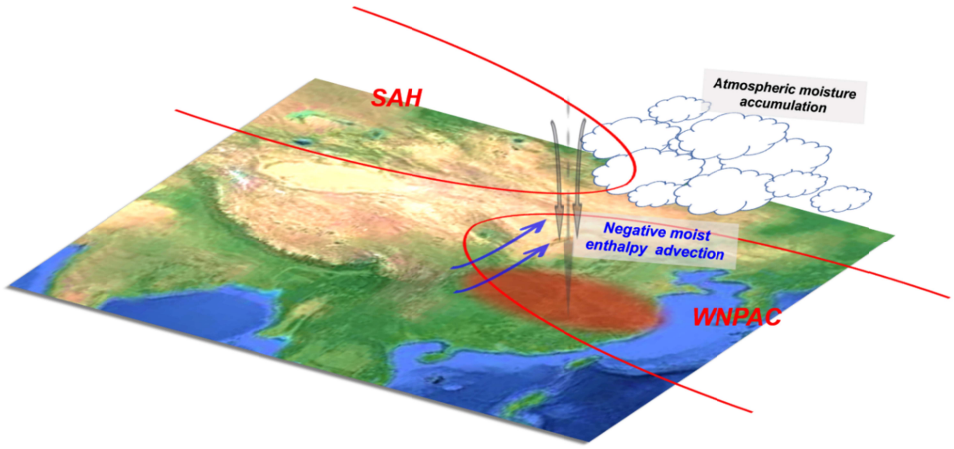

361
362 **Figure 9.** Schematic of the influence of extreme dry advection on the record-breaking Yangtze River
363 heatwave in midsummer of 2022.

364 (1) The area-averaged SAT anomalies over the YRV in midsummer of 2022 relative to the
365 1979–2021 climatology is 1.98 °C, which sets the highest record for the period 1950-2022. The
366 2022 YRV heatwave is dominated by the component of interannual variability, which
367 contributes 1.44 °C to the total temperature anomalies, accounting for 72.7% of the anomaly
368 amplitude.

369 (2) Diagnostic analysis based on the linearized surface heat budget equation indicates that
370 the anomalous surface cloud radiative forcing is the most important process dominating the 2022
371 YRV heatwave, which contributes 2.39°C to the total anomalies. The anomalous surface cloud
372 radiative forcing is dominated by the positive surface short-wave cloud radiative forcing
373 associated with the negative precipitation anomalies and associated decreased cloud cover over
374 the YRV, which is induced by the vertical dynamical processes of anomalous moisture
375 advection.

376 (3) Budget analysis of column-integrated MSE equation for the anomalous vertical velocity
377 over the YRV suggest that the anomalous descending flows are driven by the anomalous
378 meridional dry air advection, which is closely related to the unusually moisture accumulations
379 over the north of YRV. Simulations from the Lagrangian model FLEXPART exhibit that the
380 moisture anomaly over the north of YRV is mainly originated from the surface evaporation in

the YRV, implying that there could be a positive land-air feedback during the life cycle of the YRV heatwave.

Acknowledgments

This work is supported by the National Natural Science Foundation of China under Grant No. 42205039, the Guangdong Basic and Applied Basic Research Foundation (2021A1515011421), the Youth Innovation Team of China Meteorological Administration (CMA2023QN15), and the China Postdoctoral Science Foundation under Grant No. 2022T150638.

Conflict of Interest

The authors declare no competing interests.

Open Research

All datasets underlying this study can be downloaded publicly as follows:

(1) ERSSTv5 (https://www.ncei.noaa.gov/products/extended-reconstructed-sst);

(2) ERA5 (https://cds.climate.copernicus.eu/cdsapp#!/dataset/reanalysis-era5-pressure-levels-monthly-means?tab=overview);

References

Biasutti, M., Voigt, A., Boos, W. R., Braconnot, P., Hargreaves, J. C., Harrison, S. P., et al. (2018). Global energetics and local physics as drivers of past, present and future monsoons. *Nature Geoscience, 11*(6), 392-400. doi:10.1038/s41561-018-0137-1

Chen, R., & Li, X. (2023). Causes of the persistent merging of the western North Pacific subtropical high and the Iran high during late July 2022. *Climate Dynamics*. doi:10.1007/s00382-023-06678-x

Chou, C., Chiang, J. C. H., Lan, C.-W., Chung, C.-H., Liao, Y.-C., & Lee, C.-J. (2013). Increase in the range between wet and dry season precipitation. *Nature Geoscience, 6*(4), 263-267. doi:10.1038/ngeo1744

Enomoto, T., Hoskins, B. J., & Matsuda, Y. (2003). The formation mechanism of the Bonin high in August. *Quarterly Journal of the Royal Meteorological Society, 129*(587), 157-178. doi:10.1256/qj.01.211

Erdenebat, E., & Sato, T. (2018). Role of soil moisture-atmosphere feedback during high temperature events in 2002 over Northeast Eurasia. *Progress in Earth and Planetary Science, 5*(1). doi:10.1186/s40645-018-0195-4

Ha, K.-J., Seo, Y.-W., Yeo, J.-H., Timmermann, A., Chung, E.-S., Franzke, C. L. E., et al. (2022). Dynamics and characteristics of dry and moist heatwaves over East Asia. *npj Climate and Atmospheric Science, 5*(1). doi:10.1038/s41612-022-00272-4

Hersbach, H., Bell, B., Berrisford, P., Hirahara, S., Horányi, A., Muñoz-Sabater, J., et al. (2020).

The ERA5 global reanalysis. *Quarterly Journal of the Royal Meteorological Society, 146*(730), 1999-2049. doi:10.1002/qj.3803

Hu, S., Zhou, T., & Wu, B. (2021). Impact of Developing ENSO on Tibetan Plateau Summer Rainfall. *Journal of Climate, 34*(9), 3385-3400. doi:10.1175/jcli-d-20-0612.1

Huang, B. Y., Banzon, V. F., Freeman, E., Lawrimore, J., Liu, W., Peterson, T. C., et al. (2015). Extended Reconstructed Sea Surface Temperature Version 4 (ERSST.v4). Part I: Upgrades and Intercomparisons. *Journal of Climate, 28*(3), 911-930. doi:10.1175/Jcli-D-14-00006.1

Jiang, J., Liu, Y., Mao, J., & Wu, G. (2023). Extreme heatwave over Eastern China in summer 2022: the role of three oceans and local soil moisture feedback. *Environmental Research Letters, 18*(4). doi:10.1088/1748-9326/acc5fb

Liu, B., Zhu, C., Ma, S., Yan, Y., & Jiang, N. (2023). Subseasonal processes of triple extreme heatwaves over the Yangtze River Valley in 2022. *Weather and Climate Extremes, 40*. doi:10.1016/j.wace.2023.100572

Lu, J., & Cai, M. (2009). Seasonality of polar surface warming amplification in climate simulations. *Geophysical Research Letters, 36*(16). doi:10.1029/2009gl040133

Lu, R.-Y., Oh, J.-H., & Kim, B.-J. (2002). A teleconnection pattern in upper-level meridional wind over the North African and Eurasian continent in summer. *Tellus A, 54*(1), 44-55. doi:10.3402/tellusa.v54i1.12122

Lu, R., Xu, K., Chen, R., Chen, W., Li, F., & Lv, C. (2023). Heat waves in summer 2022 and increasing concern regarding heat waves in general. *Atmospheric and Oceanic Science Letters, 16*(1). doi:10.1016/j.aosl.2022.100290

Ma, M., Qu, Y., Lyu, J., Zhang, X., Su, Z., Gao, H., et al. (2022). The 2022 extreme drought in the Yangtze River Basin: Characteristics, causes and response strategies. *River, 1*(2), 162-171. doi:10.1002/rvr2.23

Mallapaty, S. (2022). China's extreme weather challenges scientists trying to study it. *Nature, 609*(7929), 888. doi:10.1038/d41586-022-02954-8

Neelin, J. D., & Held, I. M. (1987). Modeling Tropical Convergence Based on the Moist Static Energy Budget. *monthly weather review, 115*(1), 3-12. doi:10.1175/1520-0493(1987)115<0003:mtcbot>2.0.co;2

Peng, D., Zhou, T., Sun, Y., & Lin, A. (2022). Interannual Variation in Moisture Sources for the First Rainy Season in South China Estimated by the FLEXPART Model. *Journal of Climate, 35*(2), 745-761. doi:10.1175/jcli-d-21-0289.1

Peng, D., Zhou, T., & Zhang, L. (2020). Moisture Sources Associated with Precipitation during Dry and Wet Seasons over Central Asia. *Journal of Climate, 33*(24), 10755-10771. doi:10.1175/jcli-d-20-0029.1

Sodemann, H., Schwierz, C., & Wernli, H. (2008). Interannual variability of Greenland winter precipitation sources: Lagrangian moisture diagnostic and North Atlantic Oscillation influence. *Journal of Geophysical Research, 113*(D3). doi:10.1029/2007jd008503

Tang, S., Qiao, S., Wang, B., Liu, F., Feng, T., Yang, J., et al. (2023). Linkages of unprecedented 2022 Yangtze River Valley heatwaves to Pakistan flood and triple-dip La Niña. *npj Climate and Atmospheric Science, 6*(1). doi:10.1038/s41612-023-00386-3

Thompson, V., Kennedy-Asser, A. T., Vosper, E., Lo, Y. T. E., Huntingford, C., Andrews, O., et al. (2022). The 2021 western North America heat wave among the most extreme events ever recorded globally. *Sci Adv, 8*(18), eabm6860. doi:10.1126/sciadv.abm6860

Wang, W., Zhou, W., & Chen, D. (2014). Summer High Temperature Extremes in Southeast China: Bonding with the El Nino-Southern Oscillation and East Asian Summer Monsoon Coupled System. *Journal of Climate, 27*(11), 4122-4138. doi:10.1175/jcli-d-13-00545.1

Wang, Z., Luo, H., & Yang, S. (2023). Different mechanisms for the extremely hot central-eastern China in July–August 2022 from a Eurasian large-scale circulation perspective. *Environmental Research Letters, 18*(2). doi:10.1088/1748-9326/acb3e5

Wu, B., Zhou, T., & Li, T. (2017). Atmospheric Dynamic and Thermodynamic Processes Driving the Western North Pacific Anomalous Anticyclone during El Niño. Part I: Maintenance Mechanisms. *Journal of Climate, 30*(23), 9621-9635. doi:10.1175/jcli-d-16-0489.1

Yuan, Y., Liao, Z., Zhou, B., & Zhai, P. (2023). Unprecedented Hot Extremes Observed in City Clusters in China during Summer 2022. *Journal of Meteorological Research, 37*(2), 141-148. doi:10.1007/s13351-023-2184-9

Zhang, D., Chen, L., Yuan, Y., Zuo, J., & Ke, Z. (2023). Why was the heat wave in the Yangtze River valley abnormally intensified in late summer 2022? *Environmental Research Letters, 18*(3). doi:10.1088/1748-9326/acba30

Zhou, T. J., & Yu, R. C. (2005). Atmospheric water vapor transport associated with typical anomalous summer rainfall patterns in China. *Journal of Geophysical Research-Atmospheres, 110*(D8). doi:10.1029/2004jd005413